Mechanistic Study on Adsorptive Removal of *tert*-Butanethiol on Ag−Y Zeolite under Ambient Conditions

Ken-ichi Shimizu,*,† Nobumitsu Kobayashi,† Atsushi Satsuma,† Toshinori Kojima,‡ and Shigeo Satokawa‡

Department of Applied Chemistry, Graduate School of Engineering, Nagoya University, Chikusa-ku, Nagoya 464-8603, Japan, and Department of Materials and Life Science, Faculty of Science and Technology, Seikei University, 3-3-1 Kichijoji-kitamachi, Musashino-shi, Tokyo 180-8633, Japan

Received: June 9, 2006; In Final Form: August 17, 2006

The dynamics and surface chemistry of *tert*-butanethiol (TBT) adsorptive removal over silver-exchanged Y zeolite (Ag−Y) were studied under ambient conditions. Saturation uptake on Ag−Y was higher than that on H−Y and Na−Y. The structural analyses by a combination of X-ray diffraction, Ag K-edge X-ray absorption near-edge structure (XANES)/extended X-ray absorption fine structures (EXAFS), Ag L_{III}-edge XANES, S K-edge XANES, and in situ UV−vis show that the AgSH molecule, Ag_2S monomer, and Ag_4S_2 cluster are the dominant silver species in TBT-saturated Ag−Y. Dynamic changes in adsorbed intermediates, gas-phase products, and the silver sulfides were followed by in situ FTIR, mass spectroscopy and in situ UV−vis, respectively. The results show the following reaction mechanism: (1) formation of *iso*-butene and adsorbed H_2S on the Ag^+ site via C−S cleavage of hydrogen-bonded TBT initially adsorbed on the Ag^+ site; (2) conversion of the adsorbed H_2S to AgSH and H^+ on zeolite; (3) the reaction of two Ag−SH species to yield Ag_2S and H^+ on zeolite.

Introduction

Polymer electrolyte fuel cells (PEFC) are one of the most promising and clean primary power generators for stationary and mobile source applications. Pipeline natural gas is one of the most useful fuels for stationary applications of PEFC because of the existence of its supply infrastructure. Though the composition of pipeline natural gas varies by region and locality,[1] a few parts per million of sulfur-containing odorants, such as dimethyl sulfide (DMS) and *tert*-butanethiol (TBT), are generally added to natural gas fuel in order to give people warning of gas leakage. Since these sulfur compounds are a severe poison for stream reforming catalysts,[2] pipeline natural gas requires deep desulfurization before introduction to the reforming process for PEFC applications. The current hydrodesulfurization (HDS) process, involving catalytic H_2 treatment to remove organosulfur compounds as H_2S, combined with subsequent adsorption of H_2S on zinc oxide, is operated at elevated temperatures (>300 °C) and pressures (20−100 atm of H_2).[3] It is difficult to apply the HDS process to residential PEFC systems, which require quick and easy start-up, simple operation, and small reactor size.[4] Hence, a new desulfurization process for PEFC systems must feature the adsorptive removal of sulfur compounds under ambient conditions.

Activated carbon and manganese dioxide are the typical adsorbents for desulfurization of natural gas at ambient temperature,[5] though the sulfur capacity of these materials is low. Wakita et al. reported a removal of DMS and TBT from natural gas by using Na- and H-exchanged zeolites at ambient temperature.[6] However, these zeolites show significantly lowered sulfur capacity in the presence of 1 000 ppm of water.[7] Recently, Satokawa et al. reported that silver-exchanged zeolites, especially Ag−Y zeolites, were favorable adsorbents with high capacity and low leakage for the desulfurization of pipeline natural gas fuel at ambient conditions even in the presence of water vapor.[7,8] Also, several reports have demonstrated that silver-exchanged zeolites are effective for removing sulfur compounds such as DMS,[9] tetrahydrothiophene,[10] and thiophenes.[11−15] Although most practical adsorptive separations exploit van der Waals interaction between adsorbates and surfaces, it has been suggested in the above studies that the selective adsorption of an organosulfur compound can be caused by some chemical interaction. A good example was reported by a group of Yang,[11−13] who demonstrated a high thiophene capacity of a silver-exchanged zeolite due to a π-complexation between these cations and thiophenic aromatic rings. For the ability to understand the chemical interaction between organosulfur compounds and adsorption sites, Ag^+ ions, spectroscopic characterization of the adsorption complex is indispensable. Although many attempts have focused on the spectroscopic characterization of silver sulfide clusters formed by the reaction of Ag-exchanged zeolite with H_2S,[16−19] few data on the reaction with organosulfur compounds is available. On the other hand, spectroscopic studies of the chemical interaction of thiophene and H−zeolite were studied in detail.[20−23] Using several characterization techniques, Iglesia et al. showed that thiophene adsorption selectivity on H−zeolite in thiophene/toluene gas mixtures was higher than that expected from only van der Waals interactions and caused by ring-opening and oligomerization of thiophene-derived adsorbed species.[21−23]

As for the state of the adsorbed TBT on Ag−Y zeolite, Satokawa et al. reported the color change of Ag−Y (white to yellow) during TBT adsorption, which could suggest the formation of silver sulfide-like species possibly via C−S bond cleavage of TBT adspecies and subsequent Ag−S bond formation.[8] In this study, we present experimental evidence for this

* Corresponding author. Fax: +81-52-789-3193. E-mail: kshimizu@apchem.nagoya-u.ac.jp.
† Nagoya University.
‡ Seikei University.

10.1021/jp063590h CCC: $33.50
Published on Web 10/13/2006

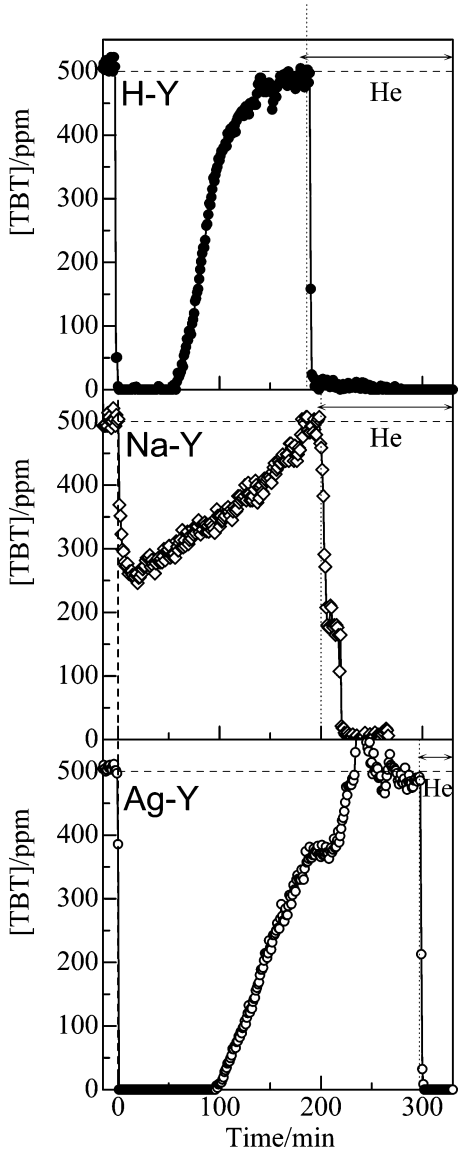

Figure 1. Breakthrough of TBT in a fixed-bed adsorber with (○) Ag−Y, (◊) Na−Y, and (●) HY, adsorbents for TBT (500 ppm)/He feed at 298 K.

hypothesis as well as the mechanism of silver sulfide formation during TBT adsorptive removal under ambient conditions. The TBT-saturated Ag−Y sample is characterized by a combination of X-ray diffraction (XRD), Ag K-edge X-ray absorption near-edge structure (XANES) and extended X-ray absorption fine structures (EXAFS), Ag L_{III}-edge XANES, S K-edge XANES, and the results show the presence of silver sulfides (AgSH, Ag_2S monomer, and Ag_4S_2 cluster). The reaction mechanism is discussed on the basis of dynamic spectroscopic data on TBT-derived surface species and gas-phase products using in situ FTIR, in situ UV−vis, and mass spectroscopy.

Experimental Section

Preparation of Adsorbents. Na−Y zeolite (JRC-Z-Y 5.6, a reference catalyst of the Catalysis Society of Japan, $SiO_2/Al_2O_3 = 5.6$, surface area = 870 $m^2\ g^{-1}$) was supplied from the Catalysis Society of Japan. Ag−Y was prepared by exchanging Na−Y with an aqueous solution of silver nitrate at 298 K for 6 h, followed by centrifuging, washing with water, and subsequent air drying at 373 K for 12 h. Silver content (15 wt %, Ag/Al = 0.6) was determined by the ICP method. Amorphous silica (JRC-SIO-8, $S_{BET} = 303\ m^2\ g^{-1}$), H−Y zeolite (JRC-Z-HY5.6, $SiO_2/Al_2O_3 = 5.6$) and Na−Y were used as reference adsorbents. Each adsorbent was crushed and sieved to obtain a particle size between 0.2 and 0.4 mm.

Adsorption Experiment. The adsorption runs were carried out in a fixed-bed flow tubular reactor (inner diameter: 3 mm). A TBT (500 ppm by volume)/He mixture was fed to adsorbents (0.2 g) at a flow rate of 100 $cm^3\ min^{-1}$ at ambient temperature (298 K) using zeolite adsorbents without any pretreatment. TBT concentrations in the reactor effluent were measured by mass spectrometry (Anelva): ionic currents of $m/e = 90$ were analyzed. To prevent changes in the operating pressure of the reactor, the excess flow from the cell was vented. Ionic currents of $m/e = 34$ and 56 in the effluent gas were also monitored, and changes in the ionic currents due to butenes ($m/e = 56$) and H_2S ($m/e = 34$) were estimated by subtracting ionic currents of $m/e = 56$ and 34 attributed to the fragmentation of TBT.

Characterization of Adsorbent. Powder X-ray diffraction patterns were taken by a Rigaku RINT 1200 X-ray diffraction meter with Cu Kα radiation. Ag K-edge X-ray absorption spectra were taken at the BL-10B station of the Photon Factory in the High Energy Accelerator Research Organization in Tsukuba (Japan), with a ring energy of 2.5 GeV and stored current of 250−350 mA. The Ag−Y sample after the adsorption experiments, named as AgY(TBT), was sealed in cells of polypropylene. The spectra were recorded in a transmission mode at room temperature with a Si(311) channel-cut monochromator. Ag L_{III}-edge and S K-edge XANES spectra were obtained at the BL-9A station of the Photon Factory with a Si(111) double-crystal monochromator using a Lytle cell and a fluorescence detector. The beam path was purged with He. High-energy X-rays from high-order reflections were removed by a pair of flat quartz mirrors coated with Rh/Ni that were aligned in parallel. The energy was defined by assigning the first inflection point of the Cu foil spectrum to 8 980.3 eV. The EXAFS data were analyzed by the EXAFS analysis program REX version 2.5. For the curve-fitting analysis of Ag−O and Ag−S shells in the Ag K-edge EXAFS, parameters extracted from Ag_2SO_4[24] and α-Ag_2S[25] were used, respectively.

In situ FTIR spectra were recorded on a JASCO FT/IR-620 equipped with the IR cell connected to a conventional flow reaction system. The sample was pressed into a 0.02-g self-supporting wafer and mounted into a quartz IR cell with CaF_2 windows. Spectra were measured with a resolution of 4 cm^{-1} at 298 K. A reference spectrum of the catalyst wafer in a flow of He was subtracted from each spectrum. Prior to each experiment the catalyst was heated in He at 373 K for 30 min, cooled to 298 K, purged for 30 min with He, and then a TBT/He gas mixture was fed at a flow rate of 100 $cm^3\ min^{-1}$.

In situ diffuse reflectance UV−vis spectra were recorded with a UV−vis spectrometer (JASCO V-550) equipped with an in situ flow cell with the quartz window used in our previous study.[26] A diffuse reflectance sample cell was connected with a gas flow system, and the light source was placed at the center of an integrating sphere by optical fiber. Reflectance was converted to pseudo-absorbance using the Kubelka−Munk function. $BaSO_4$ was used to collect a background spectrum. A TBT (500 ppm)/He gas mixture was fed to the Ag−Y sample (50 mg) at a flow rate of 100 $cm^3\ min^{-1}$, and in situ UV−vis spectra were recorded at 298 K.

Results and Discussion

Adsorption of TBT. A TBT (500 ppm)/He gas mixture was passed through a fixed-bed column, and the outlet concentration

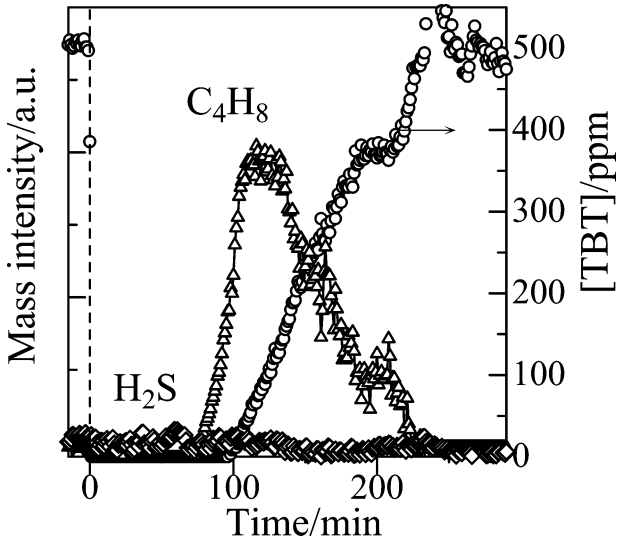

Figure 2. Changes in the mass intensities for outlet (△) C_4H_8 (m/e = 56), (◇) H_2S (m/e = 34), and (○) breakthrough of TBT during TBT (500 ppm) adsorption on Ag−Y at 298 K. Mass intensities for H_2S (m/e = 34) and C_4H_8 (m/e = 5 634) were normalized by those at t = 0 min.

of TBT was monitored as a function of time. Before introducing a TBT/He flow to the adsorbent containing column, TBT (500 ppm) was fed to the detector through a bypass line. Results are shown in Figure 1 as breakthrough curves for each adsorbent. Note that adsorbents were tested without any pretreatment, and hence physically adsorbed water is present on the adsorbents before adsorption experiments. For Ag−Y, TBT was initially depleted from inlet streams for 100 min, after which its concentration increased and ultimately reached inlet level as the adsorbent reached saturation coverage. The color of Ag−Y changed from white to yellow. The saturation adsorbed capacity of Ag−Y listed in Table 1 was estimated to be 1.8 mmol g^{-1} from a time integral of the differences between inlet and outlet concentrations. When the sample was purged with He for 33 min after saturation, weakly adsorbed TBT was desorbed, but most of the adsorbed TBT (1.78 mmol g^{-1}) remained on Ag−Y as irreversibly adsorbed TBT. The amount of desorbed TBT (0.02 mmol g^{-1}) was only 1.1% of the total uptake. The breakthrough curves for H−Y and Na−Y are shown in Figure 1. For H−Y, the breakthrough of TBT occurred earlier than Ag−Y. The breakthrough occurred immediately after flowing TBT over Na−Y. Consequently, the amount of irreversibly adsorbed TBT on Ag−Y (1.78 mmol g^{-1}) was higher than that of Na−Y (0.36 mmol g^{-1}) and H−Y (0.96 mmol g^{-1}), suggesting that the Ag^+ ion is responsible for a strong interaction with TBT-derived species. The S/Ag value, defined as the ratio of the amount of irreversibly adsorbed TBT to silver content, was 1.28 for Ag−Y.

Mass spectroscopy connected to a fixed-bed absorber was used to provide information on the gas-phase products in the reaction of TBT-derived species on Ag−Y. As shown in Figure 2, formation of butenes (m/e = 56) was observed. The mass intensity was highest around a breakthrough point, and the formation of butenes was finished when a saturation coverage of TBT on Ag−Y was achieved. It is clear that butenes, most probably *iso*-butene, were formed through dissociative adsorption of TBT with the rupture of the C−S bond. Note that no formation of H_2S (m/e = 34) was confirmed by mass spectroscopy. Taking into account the high S/Ag ratio as well as the color change after TBT adsorption, these results suggest that the desulfurization reaction of TBT with rupture of the C−S bond occurs on Ag−Y, leading to the formation of butenes and silver−sulfur compounds. This hypothesis is verified in detail by the following spectroscopic experiments.

TABLE 1: Summary of TBT Adsorption Experiments at 298 K

samples	N_t[a] mmol g^{-1}	N_r[b]	N_{irr}[c]	S/Ag[d]
Ag−Y	1.80	0.02	1.78	1.28
Na−Y	0.49	0.13	0.36	
H−Y	1.00	0.04	0.96	

[a] Total amount of adsorbed TBT. [b] Amount of reversibly adsorbed TBT. [c] Amount of irreversibly adsorbed TBT. [d] The ratio of the amount of irreversibly adsorbed TBT to silver content.

In Situ FTIR Studies. Infrared spectra of TBT-derived adsorbed species on Ag−Y, Na−Y, and SiO_2 were measured at room temperature after exposing the sample disk to a TBT (0.5%)/He mixture for 4 min, followed by purging with He for 2 min. The spectra are shown in Figure 3. The reaction pathway derived from the following characterizations is shown in Scheme 1. A ν(SH) band at 2 570 cm^{-1} observed in the spectrum of SiO_2 is assigned to physisorbed TBT, because the band completely disappeared after purging with He for 30 min. In previous IR studies of CH_3SH adsorption on metal oxides,[27,28] the ν-(SH) band at 2 570 cm^{-1} was assigned to physisorbed CH_3SH, which supports the above band assignment (2 570 cm^{-1} to physisorbed TBT). For Na−Y, two strong ν(SH) bands with lower wavenumbers (2 530, 2 560 cm^{-1}) were observed. After purging with He for 30 min, the intensity of these bands was 83% of the initial value, suggesting that the bands are assigned to irreversibly adsorbed TBT. Previously, Wakita et al.[6] reported IR spectra of TBT adspecies on Na−Y and assigned the band at 2 599 cm^{-1} to TBT coordinatedly adsorbed on Na^+ through the lone electron pair of the sulfur atom. A broad ν(SH) band at 2 500 cm^{-1} and a shoulder around 2 570 cm^{-1} were observed on the spectrum of Ag−Y after TBT adsorption. The shoulder band around 2 570 cm^{-1} is assigned to undissociatively adsorbed TBT (**1** in Scheme 1) as a minor species. In contrast to the spectra for SiO_2 and Na−Y, ν(C═C) bands assignable to olefins[29−31] and a broad band at 1 310 cm^{-1} were also observed. On the basis of previous studies, a relatively sharp band centered around 1 640−1 650 cm^{-1} can be assigned to a molecularly adsorbed *iso*-butene.[29−31] In a CH deformation region for Ag−Y, bands at 1 465, 1 454, 1 370, and 1 360 cm^{-1} due to δCH of *tert*-butyl group of absorbed TBT and/or adsorbed *iso*-butene[29−31] were observed. In previous IR studies on H_2S adsorption on Al_2O_3, bands at 2 560 $cm^{-1}$and 1 335 cm^{-1} were assigned to the S−H stretching and H−S−H bending modes of an undissociated H_2S molecule.[32−34] Therefore, broad bands at 2 500 and 1 310 cm^{-1} are assigned the ν(SH) and δ(HSH) modes of the H_2S molecule on Ag−Y (**2** in Scheme 1). The adsorption of H_2S on the Na−ZSM-5 zeolite was investigated by Garcia and Lercher, and they assigned the IR band at 2 580 cm^{-1} to H_2S adsorbed coordinatevely on the Na^+ cation via the sulfur atom.[35] Lower frequencies of ν(SH) and δ(HSH) modes for the H_2S on Ag−Y indicate the lower bond strength of S−H bonds. According to HSAB (hard soft acid and base) theory, Ag^+ ion and H_2S are respectively classified as soft acid and soft base, while Na^+ ion is a hard Lewis acid. Thus, the lower S−H bond strength of H_2S on the Ag^+ site should result from the greater interaction of the Ag^+ site as a soft Lewis acid with H_2S as a soft Lewis base. TBT saturation uptake on Na−Y zeolite significantly drops in the presence of 1 000 ppm water.[6,7] This can result from the greater interaction of Na^+ (hard Lewis acid) with water (hard Lewis base).

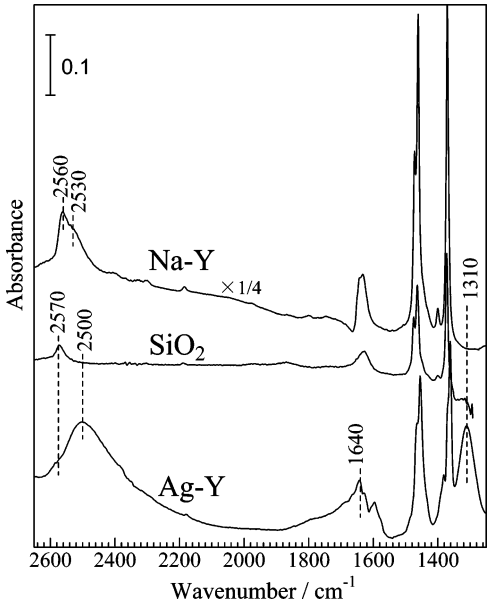

Figure 3. IR spectra of adsorbed species on various adsorbents after flowing TBT (0.5%)/He for 4 min, followed by purging with He for 2 min.

The samples, dehydrated at 373 K under He purging, contain adsorbed water. A δ(HOH) band at 1 620 cm^{-1} characteristic of molecular water was observed for each sample. We speculate that the adsorption of TBT results in the desorption of chemisorbed H_2O, and that this is the origin of this band.

Figure 4A shows changes in the IR spectra of adsorbed species on Ag−Y as a function of time for He purging. The dynamic changes in the band intensities observed in the spectra for Ag−Y are plotted in Figure 4B. Figure 4B shows that H_2S adsorbed on the Ag^+ site (1 310, 2 500 cm^{-1}) and *iso*-butene (1 640 cm^{-1}) are formed immediately after the feeding of the TBT/He mixture. After purging with He for 20 min, the shoulder band at 2 570 cm^{-1} due to undissociatively adsorbed TBT disappeared, and simultaneously the δ(HSH) and ν(SH) modes of H_2S (1 310, 2 500 cm^{-1}) increased, which indicates that undissociatively adsorbed TBT (**1** in Scheme 1) is converted to H_2S on the Ag^+ site (**2** in Scheme 1). Then, the δ(HSH) and ν(SH) modes of H_2S (1 310, 2 500 cm^{-1}) decreased with time, and a broad shoulder band around 2 300 cm^{-1} appeared. Taking into account a significantly broad feature of the latter band as well as the absence of the δ(HSH) band, the band at 2 300 cm^{-1} can be assigned to AgSH species with the acidic S−H bond (**3** in Scheme 1). It is reasonable to assume that AgSH (**3**) could be formed by S−H bond dissociation of H_2S on Ag^+ (**2**) and the simultaneous formation of H^+ on cation-exchange sites of zeolite. A group of Calzaferri et al. also proposed that the reaction of Ag^+ ion with H_2S yields the AgSH molecule and a proton. From the above results it is concluded that undissociatively adsorbed TBT (**1**) immediately undergoes C−S bond rupture with the Ag^+ site to form *iso*-butene adsorbed in the zeolite and H_2S adsorbed on a Ag^+ site (**2**) which is then converted to AgSH (**3**).

XAFS Studies on Silver Sulfides in Ag−Y. To clarify the structure of the Ag species in TBT-saturated Ag−Y, Ag−Y (0.2 g) was exposed to 500 ppm TBT for 297 min, followed by purging with He for 30 min; the obtained powder, named as Ag−Y(TBT), was characterized by XRD and XAFS as shown below. The XRD pattern of Ag−Y did not essentially change after TBT adsorption, and no lines due to Ag_2S were observed.

The structure of the X-ray amorphous species can be investigated with XAFS spectroscopy (XANES and EXAFS),

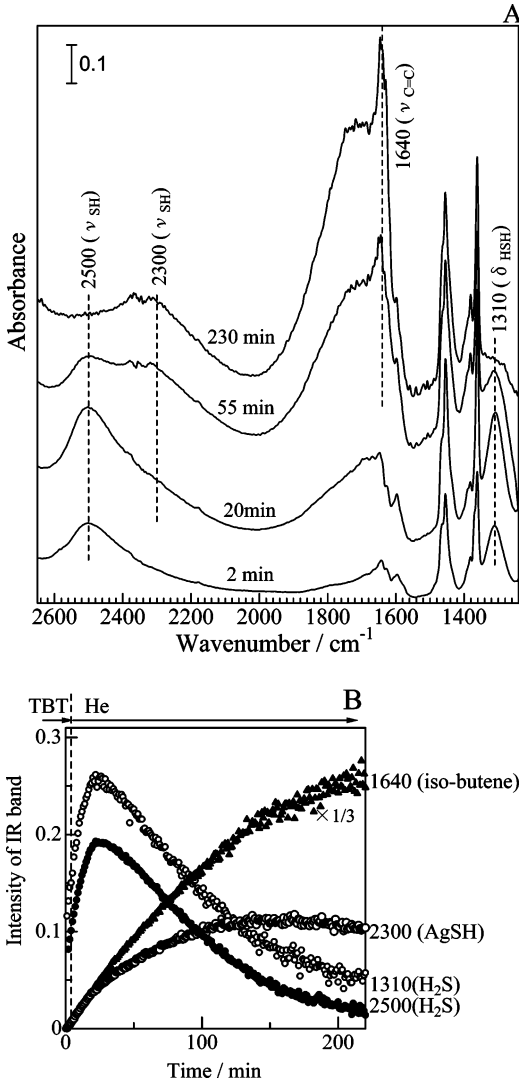

Figure 4. (A) Changes in the IR spectra of adsorbed species on Ag−Y as a function of time of He purging. Ag−Y was pre-exposed to TBT (0.5%)/He for 4 min. (B) Time course of the IR band heights.

SCHEME 1

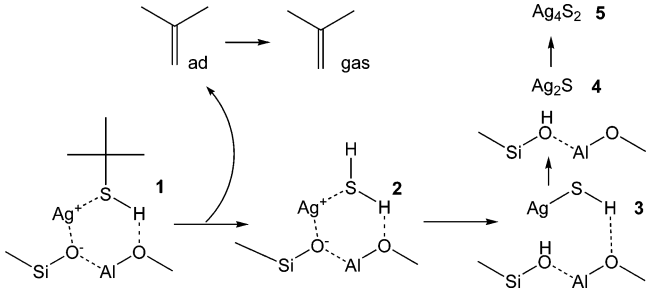

because it potentially provides average structural information of all the Ag species in the sample. As shown in Figure 5, the XANES feature of fresh Ag−Y sample was close to that of Ag_2SO_4, in which Ag^+ ions are surrounded by six oxygen atoms with an Ag−O bond distance of 2.4−2.6 Å.[24] This reflects the presence of Ag^+ ions exchanged to the cation-exchange sites of zeolite. The same conclusion is obtained from Ag L_{III}-edge XANES results shown in Figure 6. The XANES features at Ag K- and L_{III}-edges changed significantly after TBT saturation. The spectra of Ag−Y(TBT) are quite similar to those of Ag_2S. The sulfur K-edge XANES is known to be sensitive to the oxidation state and chemical environment of sulfur atoms,[36,37]

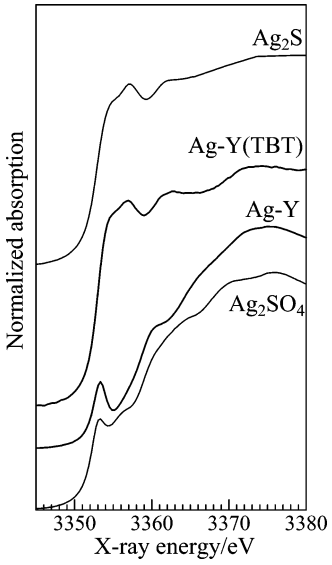

Figure 5. Ag L_{III}-edge XANES spectra of the fresh Ag−Y, TBT-saturated Ag−Y, and reference compounds.

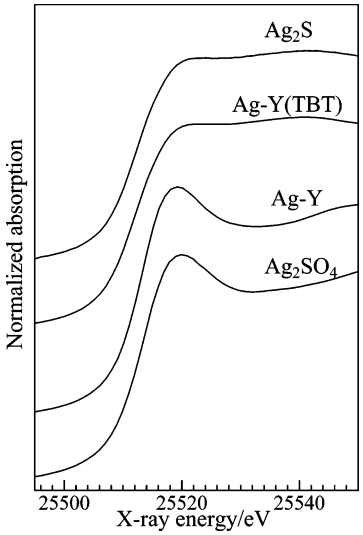

Figure 6. Ag K-edge XANES spectra of the fresh Ag−Y, TBT-saturated Ag−Y, and reference compounds.

and the S K-edge XANES spectra are shown in Figure 7 to discern the type of sulfur compounds present in Ag−Y(TBT) in comparison with those on TBT-saturated Na−Y, Na−Y(TBT). Taking into account the IR results in Figure 3, the dominant sulfur compounds present on Na−Y(TBT) should be the TBT coordinatively adsorbed on Na^+. The S K-edge XANES features for Ag−Y(TBT) are clearly different from those for Na−Y(TBT) but rather close to those of Ag_2S. From the above XRD and XANES results, it is concluded that silver sulfide clusters are the dominant silver species in TBT-saturated Ag−Y.

The Fourier transforms (FTs) of Ag K-edge EXAFS of fresh and TBT-saturated samples are shown in Figure 8. The FTs of EXAFS significantly changed after TBT saturation; an intense peak due to the first neighboring atom appeared. The EXAFS features of Ag−Y(TBT) are very close to those of Ag_2S. Curve-fitting analyses were performed for the first shell as shown in Figure 9. Simulated spectra (dotted lines), calculated using parameters of the Ag−S or Ag−O shells extracted from Ag_2S or Ag_2SO_4, respectively, fitted fairly well with the inverse Fourier transforms of k^3-weighted EXAFS (solid lines). The curve-fitting results listed in Table 2confirm the formation of

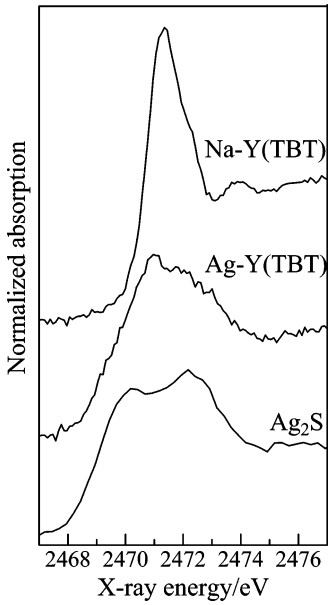

Figure 7. S K-edge XANES spectra of the TBT-saturated Na−Y, TBT-saturated Ag−Y, and Ag_2S.

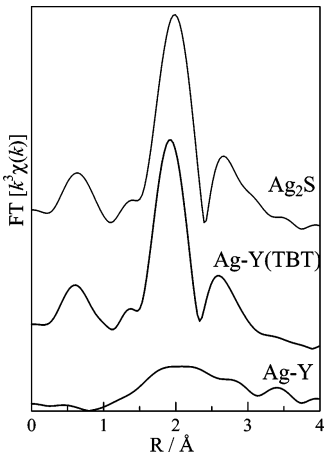

Figure 8. Fourier transforms of k^3-weighted Ag K-edge EXAFS for the fresh Ag−Y, TBT-saturated Ag−Y, and Ag_2S.

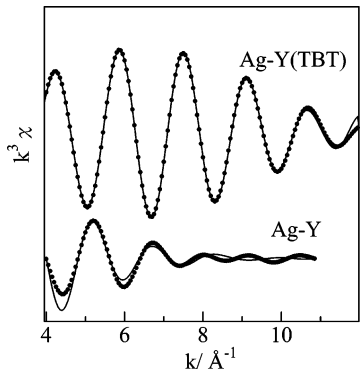

Figure 9. Fourier-filtered EXAFS functions for the first shell: experimental (solid lines) and simulated functions (dotted lines).

the Ag−S bond after the desulfurization reaction of TBT over Ag−Y. Ag−S coordination numbers of the first Ag−S shell (CN = 2.8) for Ag−Y(TBT) were smaller than those for crystalline Ag_2S (CN = 4 for α-Ag_2S), suggesting the smaller particle size of silver sulfide species in Ag−Y (TBT). In crystalline α-Ag_2S, the shortest Ag−S distances are in the range 2.42−2.40 Å and the next range of 2.57−2.60 Å.[25] The Ag−S distance of Ag−Y(TBT) sample (R = 2.45 Å) is shorter than

TABLE 2: Curve-Fitting Analysis of Ag K-edge EXAFS

samples	shell	CN[a]	*R*/Å[b]	σ^2/ Å^2 [c]	R/%[d]
Ag−Y (TBT)	S	2.8	2.45	0.037	0.3
Ag_2S	S	(4)[e]	(2.52)[e]		
Ag−Y	O	3.0	2.60	0.091	11

[a] Coordination number. [b] Bond distance. [c] Debye−Waller factor. [d] Residual factor. [e] Crystallographic values used for the curve-fitting analysis.[25]

that of crystalline α-Ag_2S and is close to that of the Ag_2S monomer estimated by quantum chemical calculation,[18] suggesting that small silver sulfide clusters, such as the Ag_2S monomer, are the dominant silver species in TBT-saturated Ag−Y.

In Situ UV−vis. Diffuse reflectance UV−vis spectroscopy has been conventionally used for the characterization of silver sulfide clusters formed by treating Ag^+-exchanged zeolite with H_2S. Calzaferri et al. reported detailed UV−vis and luminescent studies on the formation of silver sulfide clusters, such as the Ag_2S monomer and Ag_4S_2, in zeolite A.[17−19] On the basis of quantum chemical calculation, the authors showed that the electronic absorption spectrum of the Ag_2S monomer is composed of four transitions (390, 354, 325, and 300 nm with oscillator strengths of 0.26, 0.62, 0.73, and 0.30, respectively), while the spectrum of AgSH composed of a single transition at 276 nm (with oscillator strength of 0.73).[18] They also showed that a red-shift of the electronic absorption bands occurs upon interaction of Ag_2S with another Ag_2S monomer, forming an Ag_4S_2 cluster,[17] and that the spectrum of the Ag_4S_2 cluster exhibits a broad band around 440 nm.[19]

We have adopted in situ diffuse reflectance UV−vis spectroscopy to obtain kinetic information on the Ag_2S cluster formation. Figure 10A shows UV−vis spectra of Ag−Y as a function of exposure time to a TBT (500 ppm)/He flow (100 mL min^{-1}). Note that the spectrum of the fresh Ag−Y sample was subtracted from each spectrum. Time courses of the band heights at 270, 325, and 440 nm are plotted in Figure 10B. Adopting the band assignment by Calzaferri et al.,[17−19] we can discuss dynamic changes in the state of the silver sulfide species as follows. After an induction period of 6 min, a band centered around 270 nm due to the AgSH molecule (**3** in Scheme 1) appeared, indicating the formation of the AgSH molecule via certain intermediates. The formation of the AgSH molecule (**3**) via the intermediate adspecies, i.e. adsorbed TBT (**1**) and H_2S adsorbed on a Ag^+ site (**2**), shown in Figure 4 is consistent with the above UV−vis result. Then the intensity of this band increased steeply with time, and a shoulder band of around 325 nm due to the Ag_2S monomer (**4**) appeared, and after 100 min, the intensity of a shoulder band at 440 nm gradually increased with time. This result indicates the formation of Ag_2S monomers via AgSH and subsequent formation of Ag_4S_2 clusters (**5**).

Reaction Mechanism. Summarizing the kinetic results obtained by in situ IR, in situ UV−vis and mass spectroscopy, together with XAFS results, the mechanism of silver sulfides formation (Scheme 1) is described as follows. The reaction of Ag^+ ion with TBT yields the AgSH molecule (**3**, ν_{SH} = 2 300 cm^{-1}, λ_{max} = 270 nm) via TBT-derived intermediates. The intermediates are undetectable with UV−vis, but they are observed by using in situ IR (Figure 4). First, undissociatively adsorbed TBT (**1**, ν_{SH} = 2 570 cm^{-1}) undergoes C−S bond rupture with the Ag^+ site to form *iso*-butene (1 640 cm^{-1}) adsorbed in the zeolite, H_2S adsorbed on the Ag^+ site (**2**, δ_{HSH} = 1 310, ν_{SH}= 2 500 cm^{-1}), and the H^+ ion on the cation-exchange site. The reaction pathways of the silver sulfides formation can be described as follows:

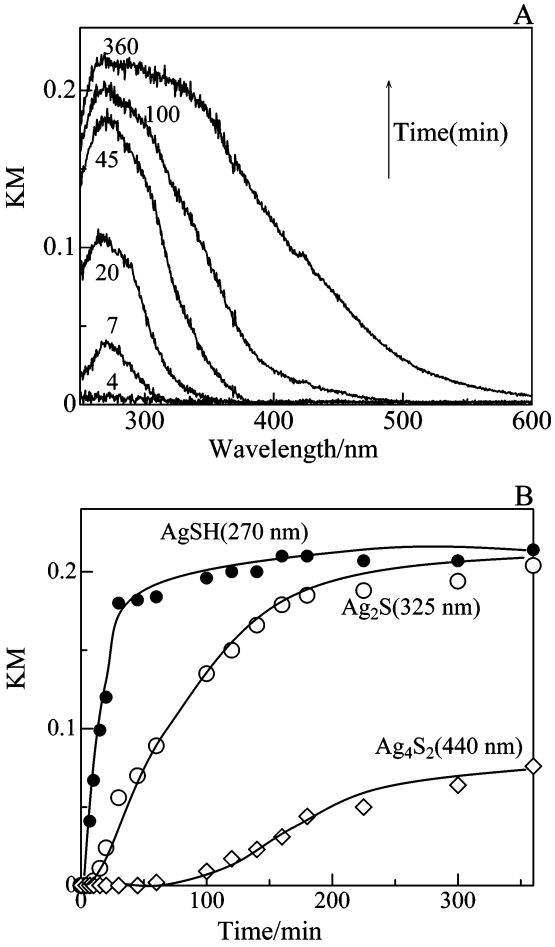

Figure 10. (A) Charges in the in situ UV−vis spectra of Ag−Y as a function of time of TBT (500 ppm)/He flowing at 298 K. (B) Increase in the height of the bands due to AgSH molecules (270 nm), Ag_2S monomers (325 nm), and Ag_4S_2 clusters (440 nm).

$$Ag^+O_Z\text{-} + H_2S \rightarrow AgSH + H^+O_Z\text{-} \quad (1)$$

$$AgSH + AgSH \rightarrow Ag_2S + H_2S \quad (2)$$

$$Ag_2S + Ag_2S \rightarrow Ag_4S_2 \quad (3)$$

As the AgSH concentration in the zeolite pore increases, the reaction of the two AgSH molecules results in the formation of the Ag_2S monomer (λ_{max} = 325 nm) and a H_2S molecule on the Ag site (**2**), which may be converted to AgSH (**3**). Finally, an increase in the concentration of Ag_2S monomers (**4**) results in dimerization of them to form Ag_4S_2 clusters (**5**) (λ_{max} = 440 nm), possibly in the super cage of the Y zeolite. When all the available Ag^+ ions are changed to silver sulfides, breakthrough occurs. Around a breakthrough point, a decrease in the pore volume caused by the formation of large Ag_4S_2 clusters may accompany the desorption of *iso*-butene adspecies as gas-phase molecules (*m*/*e* = 56). Liu et al. reported that olefins are strongly adsorbed on Ag^+ ions exchanged to zeolites.[39] Therefore, a decrease in the amount of Ag^+ sites available for *iso*-butene adsorption can also be responsible for the desorption of the *iso*-butene adspecies around the breakthrough point. The UV−vis results show the coexistence of several silver sulfides, AgSH, Ag_2S, and the Ag_4S_2 cluster, in the saturated sample (t = 360 min). The structural model of Ag−Y(TBT) derived from in situ UV−vis is basically consistent with that from XANES and

EXAFS. To our knowledge there are no experimental results on the structure of silver sulfide clusters in zeolite. The Ag−S distance of the Ag−Y(TBT) sample (R = 2.45 Å) is longer than that of the AgSH molecule estimated by quantum chemical calculation (R = 2.32 Å)[18] and is in a range of Ag−S distances for Ag_2S monomers (R = 2.42 Å)[18] and Ag_4S_2 clusters[25] estimated by quantum chemical calculation. Therefore, our EXAFS data indicates that Ag_2S monomers and Ag_4S_2 clusters are the major species and that AgSH is the minor species in Ag−Y(TBT).

The stoichiometry of the overall reaction can be described as follows:

$$2Ag^+O_Z\text{-} + C_4H_9SH \rightarrow Ag_2S + 2H^+O_Z\text{-} + C_4H_8 \quad (4)$$

$$Ag^+O_Z\text{-} + C_4H_9SH \rightarrow AgSH + H^+O_Z\text{-} + C_4H_8 \quad (5)$$

If every TBT molecule reacts with two Ag^+ ions to produce $(Ag_2S)_n$ clusters (n = 1 or 2), S/Ag should be 0.5. However, the S/Ag value for TBT-saturated Ag−Y (Table 1) was 1.28. This result can be explained by the following assumptions: (1) TBM are adsorbed on the H^+ ion on the cation-exchange site; (2) parts of the Ag species are not present as $(Ag_2S)_n$ but as AgSH. The first assumption is supported by the moderate adsorption capacity of H−Y (Table 1). The latter assumption is conceivable, if the initial distribution of silver ions in zeolite Y is taken into account. Crystallographic study[38] established that the Ag^+ ions in Ag−Y zeolite occupy three sites, site I, site I′, and site II in a ratio of 16/10.7/28.3. The Ag^+ ions at site II lie within the large cavity, whereas site I and site I′ are located in the framework.[38] Hence, we speculate that less than 50% of the Ag^+ ions, located at site I and site I′, are unavailable as an adsorption site for bulky TBT molecules, but only function as an adsorption site for H_2S intermediates, which results in the formation of Ag−SH. All the Ag^+ ions at site II can be converted to $(Ag_2S)_n$ clusters.

Conclusions

Kinetic and spectroscopic studies were performed on the mechanism of TBT adsorptive removal over Ag−Y under ambient conditions, and the following mechanism was established. The adsorbed TBT molecule on Ag^+ undergoes C−S bond rupture by the Ag^+ site, resulting in the formation of *iso*-butene adsorbed in the zeolite, H_2S adsorbed on the Ag^+ site, and H^+ ion on the cation-exchange site. As the AgSH concentration in the zeolite pore increases, the reaction of two AgSH molecules results in the formation of the Ag_2S monomer and a H^+ ion on the cation-exchange site. Finally, an increase in the concentration of the Ag_2S monomers results in dimerization of them to form Ag_4S_2 clusters in the zeolite. Around a breakthrough point, a decrease in pore volume and a decrease in the number of Ag^+ sites may accompany the desorption of *iso*-butene adspecies as gas-phase molecules. AgSH, Ag_2S monomers, and Ag_4S_2 clusters are the dominant silver species in TBT-saturated Ag−Y. Additionally, the EXAFS results of TBT-saturated Ag−Y is of importance as the first experimental results on the structure of silver sulfide clusters in zeolite.

Acknowledgment. The X-ray absorption experiments were performed under the approval of the Photon Factory Program Advisory Committee (Proposal No. 2003G-274). We thank Dr. Y. Inada of the Photon Factory for his help in the XAFS experiment.

References and Notes

(1) Farrauto, R.; Hwang, S.; Shore, L.; Ruttinger, W.; Lampert, J.; Giroux, T.; Liu, Y.; Ilinich, O. *Annu. Rev. Mater. Res.* **2003**, *33*, 1.
(2) Rostrup-Nielsen, J. R. in *Catalysis Science and Technology;* Anderson, J. R.; Boudart, M., Eds.; Springer-Verlag: Berlin, 1984; Vol. 5, p 95.
(3) Topsøe, H.; Clausen, B. S.; Massoth, F. E. In *Catalysis Science and Technology*; Anderson, J. R., Boudart, M., Eds.; Springer-Verlag: Berlin, 1996; Vol. 11.
(4) Horinouchi, H.; Osaka, N.; Miyake, J.; Kawamura, M.; Miura, T.; Nishizaki, K. *Abstracts 2003 Fuel Cell Seminar*, Miami Beach, FL, 3−7 November 2003; p 17.
(5) Futami, H.; Hashizume, Y.; *Proc. Int. Gas Res. Conf*., 1989; Gas Research Institute: Chicago, 1990; p 1592.
(6) Wakita, H.; Tachibana, Y.; Hosaka, M.; *Microporous Mesoporous Mater.* **2001**, *46*, 237.
(7) Satokawa, S.; Kobayashi, Y.; Fujiki, H. *Stud. Surf. Sci. Catal*. **2003**, *145*, 399.
(8) Satokawa, S.; Kobayashi, Y.; Fujiki, H. *Appl. Catal., B* **2005**, *56*, 51.
(9) Kasaoka, S.; Sasaoka, E.; Funahara, M. *Nihon Kagaku Kaishi* **1981**, *13*, 1945.
(10) Bezverkhyy, I.; Bouguessa, K.; Geantet, C.; Vrinat, M. *Appl. Catal., B* **2006**, *62*, 299.
(11) Hernandez-Maldonado, A. J.; Yang, R. T. *J. Am. Chem. Soc*. **2004**, *126*, 992.
(12) Hernandez-Maldonado, A. J.; Yang, R. T. *Catal. Rev*. **2004**, *46*, 111.
(13) Yang, R. T.; Hernandez-Maldonado, A. J.; Yang, F. H. *Science* **2003**, *301*, 79.
(14) McKinley, S. G.; Angelici, R. J. *Chem. Commun*. **2003**, 2620.
(15) Hayashi, A.; Saimen, H.; Watanabe, N.; Kimura, H.; Kobayashi, A.; Nakayama, H.; Tsuhako, M. *Langmuir* **2005**, *21*, 7238.
(16) Takahashi, A.; Yang, R. T.; Munson, C. L.; Chinn, D. *Ind. Eng. Chem. Res*. **2001**, *40*, 3979.
(17) Brühwiler, D.; Seifert, R.; Calzaferri, G. *J. Phys. Chem. B* **1999**, *103*, 6397.
(18) Brühwiler, D.; Leiggener, C.; Glaus, S.; Calzaferri, G. *J. Phys. Chem. B* **2002**, *106*, 3770.
(19) Leiggener, C.; Brühwiler, D.; Calzaferri, G. *J. Mater. Chem*. **2003**, *13*, 1969.
(20) Garcia, C. L.; Lercher, J. A. *J. Phys. Chem.* **1992**, *96*, 2669.
(21) Chica, A.; Strohmaier, K.; Iglesia, E. *Langmuir* **2004**, *20*, 10982.
(22) Chica, A.; Strohmaier, K.; Iglesia, E. *Appl. Catal., B* **2005**, *60*, 223.
(23) Yu, S. Y.; Garcia-Martinez, J.; Li, W. Meitzner, G. D.; Iglesia, E. *Phys. Chem. Chem. Phys.* **2002**, *4*, 1241.
(24) Brese, N. E.; O'Keeffe, M.; Ramakrishna, B. L.; Von Dreele, R. B. *J. Solid State Chem*. **1990**, *89*, 184.
(25) Bagatur'yants, A. A.; Safonov, A. A.; Stoll, H.; Werner, H. *J. Chem. Phys.* **1998**, *109*, 3096.
(26) Satsuma, A.; Shibata, J.; Wada, A.; Shinozaki, Y.; Hattori, T. *Stud. Surf. Sci. Catal*. **2002**, *145*, 235.
(27) Saur, O.; Chevreau, T.; Lamotte, J.; Travert, J.; Lavalley, J.-C. *J. Chem. Soc., Faraday Trans. 1* **1981**, *77*, 427.
(28) Travert, J.; Manoilova, O. V.; Tsyganenko, A. A.; Mauge, F.; Lavalley, J.-C. *J. Phys. Chem. B* **2002**, *106*, 1350.
(29) Ivanov, P.; Papp, H. *Langmuir* **2000**, *16*, 7769.
(30) Kondo, J. N.; Yoda, E.; Ishikawa, H.; Wakabayashi, F.; Domen, K. *J. Catal*. **2000**, *191*, 275.
(31) Trombetta, M.; Busca, G.; Rossini, S.; Piccoli, V.; Cornaro, U. *J. Catal*. **1997**, *168*, 349.
(32) Deo, A. V.; Dalla Lana, I. G. *J. Catal*. **1971**, *21*, 270.
(33) Datta, A.; Cavell, R. G. *J. Phys. Chem.* **1985**, *89*, 450.
(34) Okamoto, Y.; Oh-hara, M.; Maezawa, A.; Imanaka, T. Teranishi, S. *J. Phys. Chem*. **1986**, *90*, 2396.
(35) Garcia, C. L.; Lercher, J. A. *J. Phys. Chem*. **1992**, *96*, 2231.
(36) George, G. N.; Gorbaty, M. L. *J. Am. Chem. Soc*. **1989**, *111*, 3182.
(37) Vairavamurthy, A.; Gorbaty, M. L. *Spectrochim. Acta, Part A* **1998**, *54*, 2009.
(38) Eulenberger, G. R.; Shoemaker, D. P.; Keli, J. G. *J. Phys. Chem.* **1967**, *71*, 1812.
(39) Liu, X.; Lampert, J. K.; Arendarskiia, D. A.; Farrauto, R. J. *Appl. Catal., B* **2001**, *35*, 125.